First-Principles Prediction of Metal-Free Magnetism and Intrinsic Half-Metallicity in Graphitic Carbon Nitride

Aijun Du,[1,*] Stefano Sanvito,[2] and Sean C. Smith[3]

[1]*Centre for Computational Molecular Science, Australian Institute for Bioengineering and Nanotechnology, University of Queensland, Queensland 4072, Brisbane, Australia*

[2]*School of Physics and CRANN, Trinity College, Dublin 2, Ireland*

[3]*Centre for Nanophase Materials Sciences, Oak Ridge National Laboratory, Oak Ridge, Tennessee 37831, USA*

(Received 9 October 2011; published 11 May 2012)

Transition metal-free magnetism and half-metallicity recently has been the subject of intense research activity due to its potential in spintronics application. Here we, for the first time, demonstrate via density functional theory that the most recently experimentally realized graphitic carbon nitride (g-C_4N_3) displays a ferromagnetic ground state. Furthermore, this novel material is predicted to possess an intrinsic half-metallicity never reported to date. Our results highlight a new promising material toward realistic metal-free spintronics application.

DOI: 10.1103/PhysRevLett.108.197207 PACS numbers: 75.50.Dd, 75.20.Ck, 71.20.Nr, 73.22.Pr

Spintronics seeks to exploit the electron spin in addition to the electrical charge for logic and memory devices, and it is igniting a revolution in information processing [1]. A key challenge, a stimulating innovation in this area, is the generation of 100% spin-polarized currents at the Fermi level. A half-metal, i.e., a material which filters the current into a single spin channel, fully meets this demand [2,3]. Up to now, half-metallicity has been shown in some materials such as manganese perovskites [4], Heusler compounds [5], the metal-DNA complex [6], the transition metal doped dilute magnetic semiconductor [7], and silicon nanowire and heterostructures [8,9]. In these materials, transition metals are believed to be responsible for the half-metallicity. However, transition-metal-contained systems may not be compatible with many current matured technologies, which mainly rely on a main group semiconductor. Additionally, the large spin coupling of the transition metal atom will result in a very short spin relaxation time, greatly impacting on the performance of spintronics devices.

Recently, a single layer of graphite, i.e., 2D graphene, has attracted considerable research attention due to its unique electronic properties [10–12]. When graphene is cut into a 1D graphene nanoribbon, magnetism will be induced at the zigzag edge together with the finite size effect [13]. One interesting application in relation to the magnetism of a zigzag graphene nanoribbon is the novel half-metallicity in the presence of an electric field as predicted by the Berkeley group [14]. This has opened an exciting pathway for the development of next-generation metal-free spintronics. However, the required in-plane electric field is too strong to be obtained in experiments [14,15]. Some new strategies have been proposed to realize such metal-free half-metallicity [16–29]. Kan *et al.* and Dutta *et al.* predicted half-metallicity in an edge modified zigzag graphene nanoribbon by a small organic molecule or B/N dopants, respectively [16–19]. Although these methods are successful in showing half-metallicity in the absence of an electric field, it remains experimentally impractical because of the difficulties on the fine control positions of functional groups or the B/N dopant. Hydrogenations of graphene or an h-BN sheet have also been reported to be ferromagnetic and half-metallic [20,21], but the experimental realization of hydrogenation is still a big challenge by the current technologies because they are often formed in a random way on a host structure. Most recently, ferroelectric poly(vinylidence fluoride) is found to be physisorbed onto graphene, and the switching between half-metallic and insulating states can be achieved [22]. Hybrid C/BN nanotubes [23] have also been predicted to be half-metallic due to an intrinsic chemical potential difference between the two boundaries [24]. Our group has also reported novel half-metallicity in a finite-length nanotube nanodot [25] and vacancy contained h-BN monolayer [26]. Despite many interesting studies, metal-free half-metallicity has never yet been experimentally reported in all the predicted systems [30]. The possible reasons would be that all the theoretically predicted half-metallicity in C/BN-based compounds needs either the carefully selective doping [16–19] or a strong external electric field [14,15,25], which may make the experimental synthesis largely inaccessible.

Very recently, a novel method based on cross-linking nitrile-containing anions in ionic liquid was used by Dai's group to generate the functionalized carbon material [31]. The experimental synthesis involves the high temperature pyrolysis of ionic liquid and then the rearrangement of chemical bonds in the pyrolytic residue. The formed carbon networks possess a high content of pyrindinic structural units, pointing out a new type of graphitic carbon nitride (g-C_4N_3) material [see Fig. 1(a)]. Such a material is essentially C-doped graphitic C_3N_4 [32]. The substitution

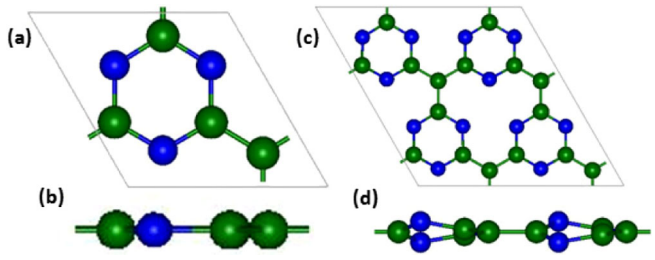

FIG. 1 (color online). (a) A top and (b) side view of the fully optimized (1×1) g-C_4N_3; (c) a top view and (d) a side view of a (2×2) reconstructed g-C_4N_3. Green and blue balls represent C and N atoms, respectively.

of the N atom with a C atom in nonmagnetic g-C_3N_4 will inject a hole into the graphitic C_3N_4 [32], which may significantly alter its electronic and magnetic properties. To explore this effect, standard density functional theory and state-of-the-art hybrid functional calculations have been carried out for the experimentally synthesized g-C_4N_3 materials. Remarkably, such a material displays a ferromagnetic ground state. Furthermore, its band structure is that of a half-metal, so that the material appears very promising for spintronics applications.

All the calculations on graphitic carbon nitride (g-C_4N_3) are performed by using the plane-wave basis Vienna *ab initio* simulation package (VASP) code [33] implementing the Perdew-Burke-Ernzerhof exchange correlation functional [34]. An all-electron description, the projector augmented wave method, is used to describe the electron-ion interaction [35]. The cutoff energy for plane waves is chosen to be 500 eV, and the vacuum space is at least 15 Å, which is large enough to avoid the interaction between periodical images. A $(7 \times 7 \times 1)$ Monkhorst-Pack grid is used for the sampling of the Brillouin zone during geometry optimization, and more than 50 K points are used to obtain the accurate band structure. All the atoms in the supercell were allowed to relax, and the convergence of force was set to 0.002 eV/Å. Spin polarization is included through all the calculations. Since standard density functional theory may fail to describe magnetism, state-of-the-art hybrid functional calculations based on the Heyd-Scuseria-Ernzerhof (HSE06) functional [36] have been also carried out to examine the magnetism and half-metallicity in a primitive g-C_4N_3 unit cell (computationally accessible).

The lattice constant of g-C_4N_3 is first calculated to be 4.84 Å. Then geometry optimization for a primitive (1×1) g-C_4N_3 is carried out by utilizing the conjugate gradient method. Figures 1(a) and 1(b) present a top and a side view of the fully relaxed (1×1) g-C_4N_3. The energy for the spin-polarized solution (ferromagnetic state) is 0.1 eV lower than that in a non-spin-polarized calculation. The magnetic moment is found to be $1\mu_B$ per formula unit, and it is evenly distributed among three neighboring nitrogen atoms in a (1×1) g-C_4N_3 as will be shown in a magnetic charge density plot [see Fig. 4(c)].

In order to explore the magnetic ground state of g-C_4N_3, an antiferromagnetic (AFM) configuration has been considered by using a (2×2) supercell. The geometry of such a supercell has been first optimized for a nonmagnetic (NM), an AFM, and a ferromagnetic (FM) configuration. Figure 2(a) presents the equilibrium configurations, local magnetic arrangements, and energetic for FM, AFM, and NM states, respectively. Clearly, the ferromagnetic state [Fig. 2(a)] is found to be the most energetically stable, with energy 0.25 and 0.23 eV lower than that of the AFM and NM configurations, respectively. The corresponding magnetic moment in a (2×2) supercell is calculated to be $4\mu_B$ for the FM state. Such ferromagnetism may be understood by the fact that the pair of electrons (occupying a C-N bonding orbital) is broken up after injecting a hole in g-C_3N_4 around the substitutional N site. Interestingly, the (2×2) g-C_4N_3 structure is found to be reconstructed into a slightly distorted structure [see Figs. 1(c) and 1(d)] during the geometry optimization. The two N-atom layers shift upward and downward with respect to the layer plane by around 0.30 Å [see Fig. 1(d)], respectively. It is important to compare the relative stability between the (1×1) and (2×2) reconstructed structures. We found that the (2×2) reconstruction is energetically more stable by 0.042 eV per (1×1) unit cell, indicating that the magnetism is robust against geometry relaxation in the supercell.

Having studied the magnetic ground state of g-C_4N_3, it is important to calculate its detailed electronic structure. Figure 3 presents the band structure and spin-resolved total density of state (TDOS) for a (1×1) unreconstructed and a (2×2) reconstructed geometry [Figs. 1(c) and 1(d)], respectively. Remarkably, the spin-up channel (red) possesses a very large band gap (~ 2 eV), whereas the spin-down one (green) did not show a gap. Thus the charge transport is

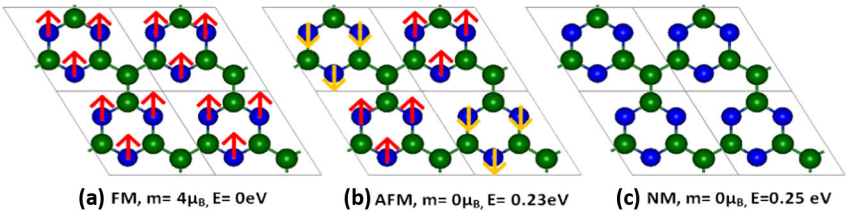

FIG. 2 (color online). Magnetic moment and relative energies for (a) FM, (b) AFM, and (c) NM states in a (2×2) reconstructed g-C_4N_3.

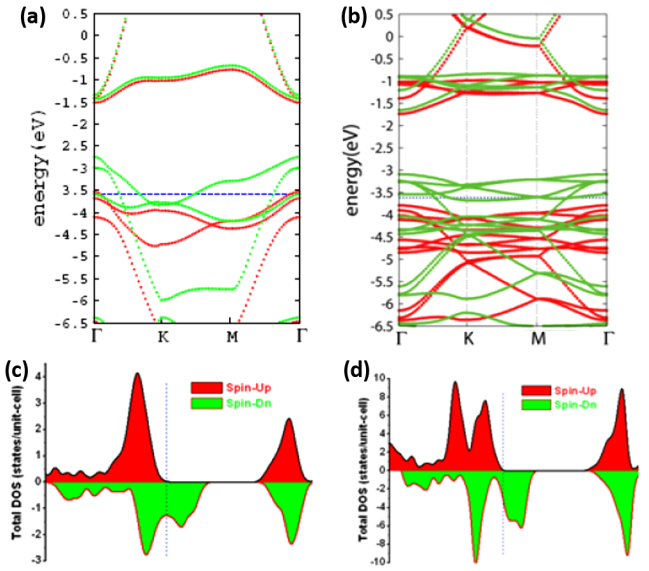

FIG. 3 (color online). Band structure and spin-resolved total density of state for a (1×1) unreconstructed [(a) and (c)] and a (2×2) reconstructed [(b) and (d)] g-C_4N_3, respectively. The short dotted line indicates the Fermi level.

dominated by the spin-down electron, and the current flow in such a system should be fully spin-polarized, i.e., half-metallicity. Additionally, close examination of the top of the valence band [see Figs. 3(a) and 3(b)] indicates that this receives contributions mainly from the planar p_y and p_x atomic orbitals.

Notably, such half-metallicity is obtained without transition metals and without external stimuli, so that g-C_4N_3 appears as the first, experimentally synthesized, metal-free half-metal.

To further understand the physical origin of ferromagnetism and half-metallicity around the Fermi level in g-C_4N_3, a detailed analysis of orbital-resolved DOS has been carried out. Figures 4(a) and 4(b) present the spin-resolved DOS projected on the p orbitals of N and C for a (1×1) unreconstructed and a (2×2) reconstructed g-C_4N_3 material, respectively. Clearly, the half-metallicity and magnetic moment are mainly attributed to the p orbital of three N atoms. Figures 4(c) and 4(d) plot top views of the 3D isosurface for net magnetic charge density (electronic charge density difference between spin-up and spin-down channel, i.e., $\rho_\uparrow - \rho_\downarrow$) in a XOY plane. Similar to a (1×1) unreconstructed g-C_4N_3, the magnetic moments are also localized around N atoms in a (2×2) reconstructed g-C_4N_3.

It is important to examine whether the experimentally fabricated g-C_4N_3 material is stable and whether the magnetic state survives at room temperature. In order to explore this aspect, a large (4×4) supercell containing 112 atoms is built, and spin-polarized *ab initio* molecular dynamics simulations are performed with a Nose-Hoover thermostat at either 300 or 500 K. Figures 5(a) and 5(b) show, respectively, the fluctuations in the temperature and the magnetic moment as a function of the simulation time at 300 K. After 30 ps, we find no structure destruction of the g-C_4N_3 monolayer. This can be understood by the fact that the binding energies of the C-N and C-C bonds are much larger than the thermal energy corresponding to room temperature. Remarkably, the ground state remains magnetic with an average magnetic moment of around $13\mu_B$ at 300 K.

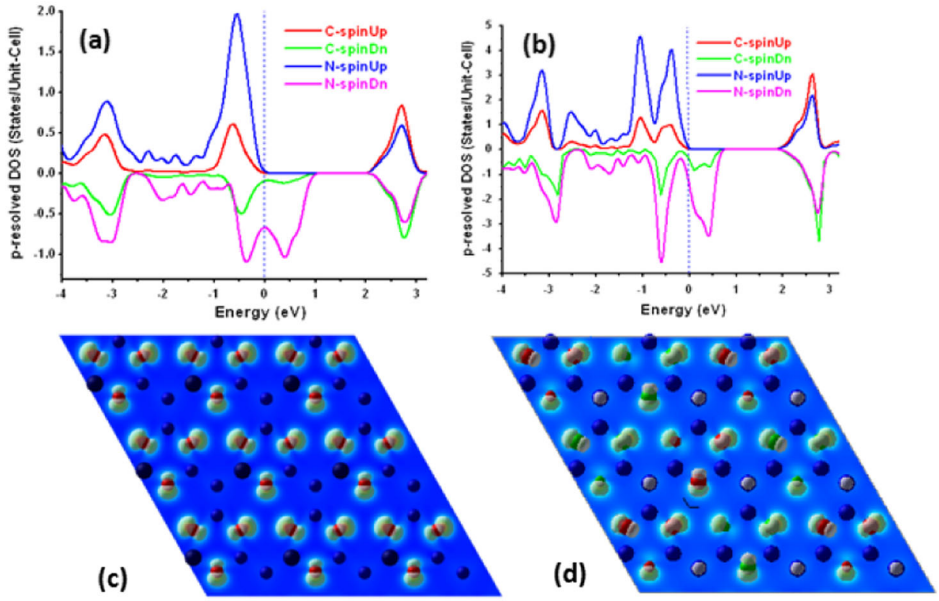

FIG. 4 (color online). Projected DOS on the p orbital of N and C atoms (a) and (b) and 3D isosurface plots of magnetic charge density $(\rho_\uparrow - \rho_\downarrow)$ for a (1×1) unreconstructed (a) and a (2×2) reconstructed (b) g-C_4N_3 in the FM ground state. The short dotted line indicates the Fermi level.

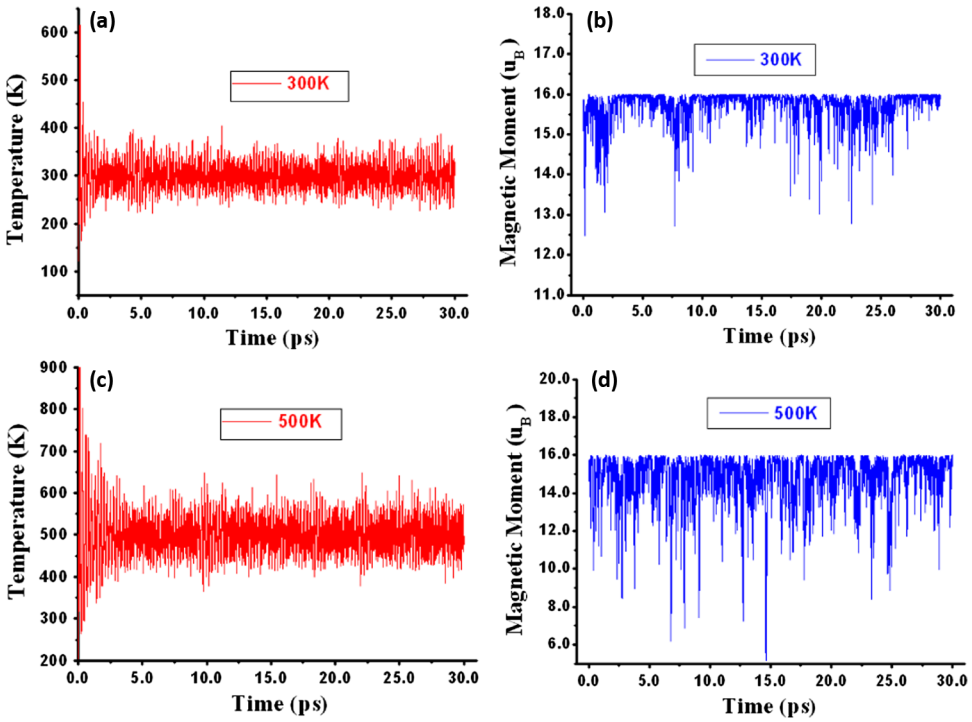

FIG. 5 (color online). The fluctuations of temperature (a) and ferromagnetic moment (b) as a function of the molecular dynamic simulation step at 300 K. (c) and (d) are similar to (a) and (b), respectively, but for another molecular dynamic run at 500 K.

Note, however, that such a temperature does not correspond to a magnetic critical temperature, as our molecular dynamics does not include spin-dynamics. As such, our result simply establishes how robust the magnetic moment is against lattice deformation. Similar structural and magnetic stability is achieved in molecular dynamics simulations at 500 K [shown in Figs. 5(c) and 5(d)].

It is well known that the general gradient approximation (Perdew-Burke-Ernzerhof exchange correlation functional) will significantly underestimate the size of the band gap. A hybrid functional such as HSE06 [36] is expected to perform very well in predicting the accurate gap and magnetic moment. Our previous work indicates that a band gap difference between density functional theory and hybrid functional methods can be as large as 1 eV in carbon-based materials [37]. To explore this effect, state-of-the-art HSE06 functional calculations have been carried out for a (1×1) unreconstructed g-C_4N_3 system, which is largely computationally accessible. Figures 6(a) and 6(b) present the calculated band structures and DOS, respectively. Clearly, both functionals predicted similar dispersion curves for valence and conduction bands, respectively, but the position of conduction bands is significantly up-shifted. Remarkably, we find that the ground state still remains ferromagnetic with the same magnetic moment ($1\mu_B$) as that obtained by the Perdew-Burke-Ernzerhof exchange

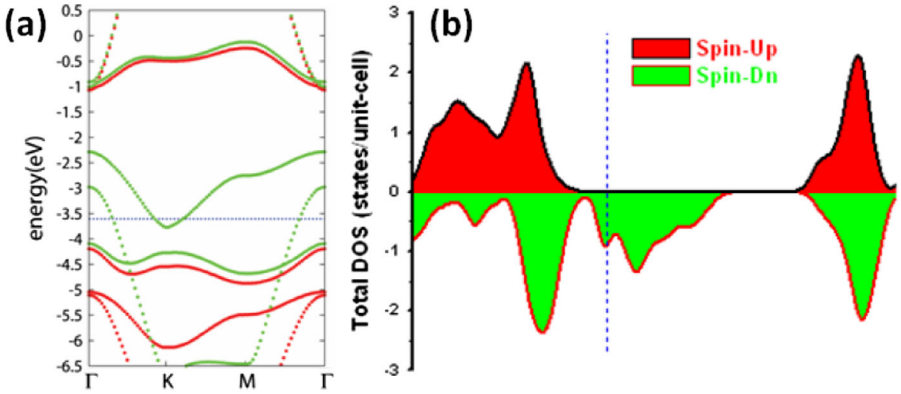

FIG. 6 (color online). (a) Band structures and (b) DOS calculated by the HSE06 functional for a (1×1) g-C_4N_3. The short dotted line indicates the Fermi level.

correlation functional (see Fig. 3). So the predicted intrinsic half-metallicity and ferromagnetism survive to the choice of functional.

In conclusion, based on first-principles simulations, we for the first time predicted that the most recently experimentally realized g-C_4N_3 material [31] exhibits a ferromagnetic ground state and intrinsic half-metallicity. Here we should note that previously proposed strategies to realize metal-free half-metallicity may be hard to be experimentally controllable, because a strong external electric field or carefully selective doping is required. Our work thus reports on the first metal-free real half-metallic material, even though the experimental synthesis of pure g-C_4N_3 may still remain a challenge. As metal-free magnets potentially offer large spin relaxation times due to small spin-orbit coupling [38], our results highlight a new promising material for experimental validation studies toward the realistic metal-free spintronics application.

We acknowledge generous grants of high-performance computer time from the AIBN cluster computing facility at The University of Queensland and the Australian Research Council (LIEF Grant No. LE0882357: A Computational Facility for Multiscale Modeling in Computational Bio and Nanotechnology), Queensland Cyber Infrastructure Foundation (QCIF), and the Australian Partnership for Advanced Computing National Facility. A. D. also greatly appreciates financial support of the Australian Research Council under Discovery Project (DP110101239). S. S. acknowledges Science Foundation of Ireland for financial support (07/IN.1/I945). S. C. S. acknowledges support from the Center for Nanophase Materials Sciences, which is sponsored at the Oak Ridge National Laboratory by the Scientific User Facilities Division, U.S. Department of Energy.

*Corresponding author.
a.du@uq.edu.au

[1] S. A. Wolf, D. D. Awschalom, R. A. Buhrman, J. M. Daughton, S. von Molnár, M. L. Roukes, A. Y. Chtchelkanova, and D. M. Treger, Science **294**, 1488 (2001).
[2] D. D. Awschalom and M. E. Flatt, Nature Phys. **3**, 153 (2007).
[3] C. Felser, G. H. Fecher, and B. Balke, Angew. Chem., Int. Ed. **46**, 668 (2007).
[4] J.-H. Park, E. Vescovo, H.-J. Kim, C. Kwon, R. Ramesh, and T. Venkatesan, Nature (London) **392**, 794 (1998).
[5] R. A. de Groot, F. M. Mueller, P. G. vanEngen, and K. H. J. Buschow, Phys. Rev. Lett. **50**, 2024 (1983).
[6] S. S. Mallajosyula and S. K. Pati, J. Phys. Chem. B **111**, 13 877 (2007).
[7] J. E. Medvedeva, A. J. Freeman, X. Y. Cui, C. Stampfl, and N. Newman, Phys. Rev. Lett. **94**, 146602 (2005).
[8] H. Wu, P. Kratzer, and M. Scheffler, Phys. Rev. Lett. **98**, 117202 (2007).
[9] E. Durgun, D. Cakir, N. Akman, and S. Ciraci, Phys. Rev. Lett. **99**, 256806 (2007).
[10] K. S. Novoselov, D. Jiang, F. Schedin, T. J. Booth, V. V. Khotkevich, S. V. Morozov, and A. K. Geim, Proc. Natl. Acad. Sci. U.S.A. **102**, 10 451 (2005).
[11] A. K. Geim and K. S. Novoselov, Nature Mater. **6**, 183 (2007).
[12] K. S. Novoselov, A. K. Geim, S. V. Morozov, D. Jiang, M. I. Katsnelson, I. V. Grigorieva, S. V. Dubonos, and A. A. Firsov, Nature (London) **438**, 197 (2005).
[13] Y. W. Son, M. L. Cohen, and S. G. Louie, Phys. Rev. Lett. **97**, 216803 (2006).
[14] Y. W. Son, M. L. Cohen, and S. G. Louie, Nature (London) **444**, 347 (2006).
[15] E. J. Kan, Z. Y. Li, J. L. Yang, and J. G. Hou, Appl. Phys. Lett. **91**, 243116 (2007).
[16] E. Kan, Z. Li, J. Yang, and J. G. Hou, J. Am. Chem. Soc. **130**, 4224 (2008).
[17] S. Dutta, A. K. Manna, and S. K. Pati, Phys. Rev. Lett. **102**, 096601 (2009).
[18] S. Dutta and S. K. Pati, J. Phys. Chem. B **112**, 1333 (2008).
[19] Y. F. Li, Z. Zhou, P. W. Shen, and Z. F. Chen, ACS Nano **3**, 1952 (2009).
[20] J. Zhou, Q. Wang, Q. Sun, X. S. Chen, Y. Kawazoe, and P. Jena, Nano Lett. **9**, 3867 (2009).
[21] W. Chen, Y. Li, G. Yu, C.-Z. Li, S. B. Zhang, Z. Zhou, and Z. Chen, J. Am. Chem. Soc. **132**, 1699 (2010).
[22] Y. L. Lee, S. Kim, C. Park, J. Ihm, and Y. W. Son, ACS Nano **4**, 1345 (2010).
[23] A. J. Du, Y. Chen, Z. H. Zhu, G. Q. Lu, and S. C. Smith, J. Am. Chem. Soc. **131**, 1682 (2009).
[24] B. Huang, C. Si, H. Lee, L. Zhao, J. Wu, B.-L. Gu, and W. Duan, Appl. Phys. Lett. **97**, 043115 (2010).
[25] A. J. Du, Y. Chen, G. Q. Lu, and S. C. Smith, Appl. Phys. Lett. **93**, 073102 (2008).
[26] A. J. Du, Y. Chen, Z. H. Zhu, R. Amal, G. Q. Lu, and S. C. Smith, J. Am. Chem. Soc. **131**, 17 354 (2009).
[27] E. J. Kan, X. J. Wu, Z. Y. Li, X. C. Zeng, J. L. Yang, and J. G. Hou, J. Chem. Phys. **129**, 084712 (2008).
[28] F. W. Zheng, G. Zhou, Z. Liu, J. Wu, W. Duan, B.-L. Gu, and S. B. Zhang, Phys. Rev. B **78**, 205415 (2008).
[29] B. Huang, C. Si, H. Lee, L. Zhao, J. Wu, B.-L. Gu, and W. Duan, Appl. Phys. Lett. **97**, 043115 (2010).
[30] A. J. Du and S. C. Smith, J. Phys. Chem. Lett. **2**, 73 (2011).
[31] J. S. Lee, X. Q. Wang, H. M. Luo, and S. Dai, Adv. Mater. **22**, 1004 (2010).
[32] E. Kroke, M. Schwarz, E. Horath-Bordon, P. Kroll, B. Noll, and A. D. Norman, New J. Chem. **26**, 508 (2002).
[33] G. Kresse and J. Furthmuller, Comput. Mater. Sci. **6**, 15 (1996); Phys. Rev. B **54**, 11 169 (1996).
[34] J. P. Perdew, K. Burke, and M. Ernzerhof, Phys. Rev. Lett. **77**, 3865 (1996).
[35] G. Kresse and D. Joubert, Phys. Rev. B **59**, 1758 (1999); P. E. Blochl, Phys. Rev. B **50**, 17 953 (1994).
[36] J. Heyd, G. E. Scuseria, and M. Ernzerhof, J. Chem. Phys. **124**, 219906 (2006).
[37] A. J. Du, Z. H. Zhu, and S. C. Smith, J. Am. Chem. Soc. **132**, 2876 (2010).
[38] S. Sanvito, Chem. Soc. Rev. **40**, 3336 (2011).